OmniH2O: Universal and Dexterous Human-to-Humanoid Whole-Body Teleoperation and Learning

Tairan He[1†] Zhengyi Luo[1†] Xialin He[2†] Wenli Xiao[1] Chong Zhang[1]
Weinan Zhang[2] Kris Kitani[1] Changliu Liu[1] Guanya Shi[1]
[1]Carnegie Mellon University [2]Shanghai Jiao Tong University [†]Equal Contributions
Page: https://omni.human2humanoid.com/

***Abstract*—We present OmniH2O (Omni Human-to-Humanoid), a learning-based system for whole-body humanoid teleoperation and autonomy. Using kinematic pose as a universal control interface, OmniH2O enables various ways for a human to control a full-sized humanoid with dexterous hands, including using real-time teleoperation through VR headset, verbal instruction, and RGB camera. OmniH2O also enables full autonomy by learning from teleoperated demonstrations or integrating with frontier models such as GPT-4o. OmniH2O demonstrates versatility and dexterity in various real-world whole-body tasks through teleoperation or autonomy, such as playing multiple sports, moving and manipulating objects, and interacting with humans. We develop an RL-based sim-to-real pipeline, which involves large-scale retargeting and augmentation of human motion datasets, learning a real-world deployable policy with sparse sensor input by imitating a privileged teacher policy, and reward designs to enhance robustness and stability. We release the first humanoid whole-body control dataset, *OmniH2O-6*, containing six everyday tasks, and demonstrate humanoid whole-body skill learning from teleoperated datasets.**

I. Introduction

How can we best unlock humanoid's potential as one of the most promising physical embodiments of general intelligence? Inspired by the recent success of pretrained vision and language models [1], one potential answer is to collect large-scale human demonstration data in the real world and learn humanoid skills from it. The embodiment alignment between humanoids and humans not only makes the humanoid a potential generalist platform but also enables the seamless integration of human cognitive skills for scalable data collections [7, 12, 29, 9].

However, *whole-body control* of a full-sized humanoid robot is challenging [21], with many existing works focusing only on the lower body [31, 17, 8, 6, 25, 24, 18] or decoupled lower and upper body control [11, 29, 22]. To simultaneously support stable dexterous manipulation and robust locomotion, the controller must coordinate the lower and upper bodies in unison. For the humanoid *teleoperation interface* [7], the need for expensive setups such as motion captures and exoskeletons also hinders large-scale humanoid data collection. In short, we need a robust control policy that *supports whole-body dexterous loco-manipulation*, while seamlessly integrating with *easy-to-use and accessible teleoperation interfaces* (e.g., VR) to enable scalable demonstration data collection.

In this work, we propose OmniH2O, a learning-based system for whole-body humanoid teleoperation and autonomy. We propose a pipeline to train a robust whole-body motion imitation policy via teach-student distillation and identify key factors in obtaining a stable control policy that supports dexterous manipulation. For instance, we find these elements to be essential: *motion data distribution*, *reward designs*, and *state space design* and *history utilization*. The distribution of the motion imitation dataset needs to be biased toward standing and squatting to help the policy learn to stabilize the lower body during manipulation. Regularization rewards are used to shape the desired motion but need to be applied with a curriculum. The input history could replace the global linear velocity, an essential input in previous work [12] that requires Motion Capture (MoCap) to obtain. We also carefully design our control interface and choose the kinematic pose as an intermediate representation to bridge between human instructions and humanoid actuation. This interface makes our control framework compatible with many real-world input sources, such as VR, RGB cameras, and autonomous agents (GPT-4o). Powered by our robust control policy, we demonstrate teleoperating humanoids to perform various daily tasks (racket swinging, flower watering, brush writing, squatting and picking, boxing, basket delivery, *etc.*). Through teleoperation, we collect a dataset of our humanoid completing six tasks such as hammer catching, basket picking, *etc.*, annotated with paired first-person RGBD camera views, control input, and whole-body motor actions. Based on the dataset, we showcase training autonomous policies via imitation learning.

In conclusion, our contributions are as follows: **(1)** We propose a pipeline to train a robust humanoid control policy that supports whole-body dexterous loco-manipulation with a universal interface that enables versatile human control and autonomy. **(2)** Experiments of large-scale motion tracking in simulation and the real world validate the superior motion imitation capability of OmniH2O. **(3)** We contribute the first humanoid loco-manipulation dataset and evaluate imitation learning methods on it to demonstrate humanoid whole-body skill learning from teleoperated datasets.

II. Universal and Dexterous Human-to-Humanoid

Problem Formulation. We formulate the learning problem as goal-conditioned RL for a Markov Decision Process (MDP) defined by the tuple $\mathcal{M} = \langle \mathcal{S}, \mathcal{A}, \mathcal{T}, \mathcal{R}, \gamma \rangle$ of state $\mathcal{S}$, action $\boldsymbol{a}_t \in \mathcal{A}$, transition $\mathcal{T}$, reward function $\mathcal{R}$, and discount factor γ. The state $\boldsymbol{s}_t$ contains the proprioception $\boldsymbol{s}^{\mathrm{p}}_t$ and the goal state $\boldsymbol{s}^{\mathrm{g}}_t$. The goal state $\boldsymbol{s}^{\mathrm{g}}_t$ includes the motion goals from the human teleoperator or autonomous agents. Based on proprioception $\boldsymbol{s}^{\mathrm{p}}_t$, goal state $\boldsymbol{s}^{\mathrm{g}}_t$, and action $\boldsymbol{a}_t$, we define the reward $r_t = \mathcal{R}\left(\boldsymbol{s}^{\mathrm{p}}_t, \boldsymbol{s}^{\mathrm{g}}_t, \boldsymbol{a}_t\right)$. The action $\boldsymbol{a}_t$ specifies the target joint angles and a PD controller actuates the motors. We apply the Proximal Policy Optimization algorithm (PPO) [28] to maximize the cumulative discounted reward $\mathbb{E}\left[\sum_{t=1}^{T} \gamma^{t-1} r_t\right]$. In this work, we study the motion imitation task where our policy π_{OmniH2O} is trained to track real-time motion input as shown in Figure 2. This task provides a universal interface for humanoid control as the kinematic pose can be provided by many different sources. We define kinematic pose as $\boldsymbol{q}_t \triangleq (\boldsymbol{\theta}_t, \boldsymbol{p}_t)$, consisting of 3D joint rotations $\boldsymbol{\theta}_t$ and positions $\boldsymbol{p}_t$ of all joints on the humanoid. To define velocities $\dot{\boldsymbol{q}}_{1:T}$, we have $\dot{\boldsymbol{q}}_t \triangleq (\boldsymbol{\omega}_t, \boldsymbol{v}_t)$ as angular $\boldsymbol{\omega}_t$ and linear velocities $\boldsymbol{v}_t$.

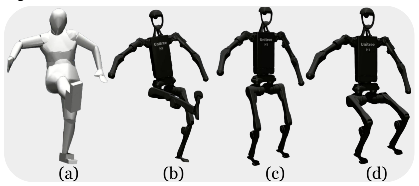

Fig. 1: (a) Source motion; (b) Retargeted motion; (c) Standing variant; (d) Squatting variant.

Human Motion Retargeting. We train our motion imitation policy using retargeted motions from the AMASS [20] dataset, using a similar retargeting process as H2O [12]. One major drawback of H2O is that the humanoid tends to take small adjustment steps instead of standing still. In order to enhance the ability of stable standing and squatting, we bias our training data by adding sequences that contain fixed lower body motion. For each motion sequence $\hat{\boldsymbol{q}}_{1:T}$ from our dataset, we create a "stable" version $\hat{\boldsymbol{q}}^{\text{stable}}_{1:T}$ by fixing the root position and the lower body to a standing or squatting position as shown in Fig. 1. We provide ablation of this strategy in Section XII.

Teacher: Privileged Imitation Policy. During real-world teleoperation of a humanoid robot, much information that is accessible in simulation (*eg.*, the global linear/angular velocity of every body link) is not available. Moreover, the input to a teleoperation system could be *sparse* (*eg.*, for VR-based teleoperation, only the hands and head's poses are known), which makes the RL optimization challenging. To tackle this issue, We first train a teacher policy that uses privileged state information and then distill it to a student policy with limited state space. Having access to the privileged state can help RL find more optimal solutions, as shown in prior works [16] and our experiments (Section III). Formally, we train a privileged motion imitator $\pi_{\text{privileged}}(\boldsymbol{a}_t | \boldsymbol{s}^{\text{p-privileged}}_t, \boldsymbol{s}^{\text{g-privileged}}_t)$, as described in Figure 2. The proprioception is defined as $\boldsymbol{s}^{\text{p-privileged}}_t \triangleq [\boldsymbol{p}_t, \boldsymbol{\theta}_t, \dot{\boldsymbol{q}}_t, \boldsymbol{\omega}_t, \boldsymbol{a}_{t-1}]$, which contains the humanoid rigidbody position $\boldsymbol{p}_t$, orientation $\boldsymbol{\theta}_t$, linear velocity $\dot{\boldsymbol{q}}_t$, angular velocity $\boldsymbol{\omega}_t$, and the previous action $\boldsymbol{a}_{t-1}$. The goal state is defined as $\boldsymbol{s}^{\text{g-privileged}}_t \triangleq [\hat{\boldsymbol{\theta}}_{t+1} \ominus \boldsymbol{\theta}_t, \hat{\boldsymbol{p}}_{t+1} - \boldsymbol{p}_t, \hat{\boldsymbol{v}}_{t+1} - \boldsymbol{v}_t, \hat{\boldsymbol{\omega}}_t - \boldsymbol{\omega}_t, \hat{\boldsymbol{\theta}}_{t+1}, \hat{\boldsymbol{p}}_{t+1}]$, which contains the reference pose $(\hat{\boldsymbol{\theta}}_t, \hat{\boldsymbol{p}}_t)$ and one-frame difference between the reference and current state for all rigid bodies of the humanoid.

Student: Sim-to-Real Imitation Policy with History. We design our control policy to be compatible with many input sources by using the kinematic reference motion as the intermediate representation. As estimating full-body motion $\tilde{\boldsymbol{q}}_t$ (both rotation and translation) is difficult (especially from VR headsets), we opt to control our humanoid with position $\tilde{\boldsymbol{p}}_t$ only for teleoperation. Specifically, for real-world teleoperation, the goal state is $\boldsymbol{s}^{\text{g-real}}_t \triangleq (\tilde{\boldsymbol{p}}^{\text{real}}_t - \boldsymbol{p}^{\text{real}}_t, \tilde{\boldsymbol{v}}^{\text{real}}_t - \boldsymbol{v}^{\text{real}}_t, \tilde{\boldsymbol{p}}^{\text{real}}_t)$. The superscript $^{\text{real}}$ indicates using the 3-points available (head and hands) from the VR headset. For other control interfaces (e.g., RGB, language), we use the same input 3-point input to maintain consistency, though can be easily extended to more keypoints to alleviate ambiguity. For proprioception, the student policy $\boldsymbol{s}^{\text{p-real}}_t \triangleq (\boldsymbol{d}_{t-25:t}, \dot{\boldsymbol{d}}_{t-25:t}, \boldsymbol{\omega}^{\text{root}}_{t-25:t}, \boldsymbol{g}_{t-25:t}, \boldsymbol{a}_{t-25-1:t-1})$ uses values easily accessible in the real-world, which includes 25-step history of joint (DoF) position $\boldsymbol{d}_{t-25:t}$, joint velocity $\dot{\boldsymbol{d}}_{t-25:t}$, root angular velocity $\boldsymbol{\omega}^{\text{root}}_{t-25:t}$, root gravity $\boldsymbol{g}_{t-25:t}$, and previous actions $\boldsymbol{a}_{t-25-1:t-1}$. The inclusion of history data helps improve the robustness of the policy with our teacher-student supervised learning. Note that no global linear velocity $\boldsymbol{v}_t$ information is included in our observations and the policy implicitly learns velocity using history information. This removes the need for MoCap as in H2O [12] and further enhances the feasibility of in-the-wild deployment.

Policy Distillation. We train our deployable teleoperation policy π_{OmniH2O} following the DAgger [26] framework: for each episode, we roll out the student policy $\pi_{\text{OmniH2O}}(\boldsymbol{a}_t | \boldsymbol{s}^{\text{p-real}}_t, \boldsymbol{s}^{\text{g-real}}_t)$ in simulation to obtain trajectories of $(\boldsymbol{s}^{\text{p-real}}_{1:T}, \boldsymbol{s}^{\text{g-real}}_{1:T})$. Using the reference pose $\hat{\boldsymbol{q}}_{1:T}$ and simulated humanoid states $\boldsymbol{s}^{\text{p}}_{1:T}$, we can compute the privileged states $\boldsymbol{s}^{\text{g-privileged}}_t, \boldsymbol{s}^{\text{p-privileged}}_t \leftarrow (\boldsymbol{s}^{\text{p}}_t, \hat{\boldsymbol{q}}_{t+1})$. Then, using the pair $(\boldsymbol{s}^{\text{p-privileged}}_t, \boldsymbol{s}^{\text{g-privileged}}_t)$, we query the teacher $\pi_{\text{privileged}}(\boldsymbol{a}_t{}^{\text{privileged}} | \boldsymbol{s}^{\text{p-privileged}}_t, \boldsymbol{s}^{\text{g-privileged}}_t)$ to calculate the reference action $\boldsymbol{a}_t{}^{\text{privileged}}$. To update π_{OmniH2O}, the loss is: $\mathcal{L} = \|\boldsymbol{a}_t{}^{\text{privileged}} - \boldsymbol{a}_t\|^2_2$.

Dexterous Hands Control. As shown in Figure 2(c), we use the hand poses estimated by VR [3, 23], and directly compute joint targets based on inverse kinematics for an off-the-shelf low-level hand controller. We use VR for the dexterous hand control in this work, but the hand pose estimation could be replaced by other interfaces (e.g., MoCap gloves [30] or RGB cameras [10]) as well.

III. Experimental Results

In our experiments, we aim to answer the following questions. **Q1.** (Section III-A) Can OmniH2O accurately track motion in simulation and real world? **Q2.** (Section III-B) Does OmniH2O support versatile control interfaces in the real world and unlock new capabilities of loco-manipulation? **Q3.** (Section III-C) Can we use OmniH2O to collect data and learn autonomous agents from teleoperated demonstrations? As motion is best seen in videos, we provide visual evaluations in our `website`.

A. Whole-body Motion Tracking

Experiment Setup. To answer **Q1**, we evaluate OmniH2O on motion tracking in simulation and the real world. In simulation, we evaluate on the retargeted AMASS dataset with augmented motions $\hat{\boldsymbol{Q}}$ (14k sequences); in real-world, we test

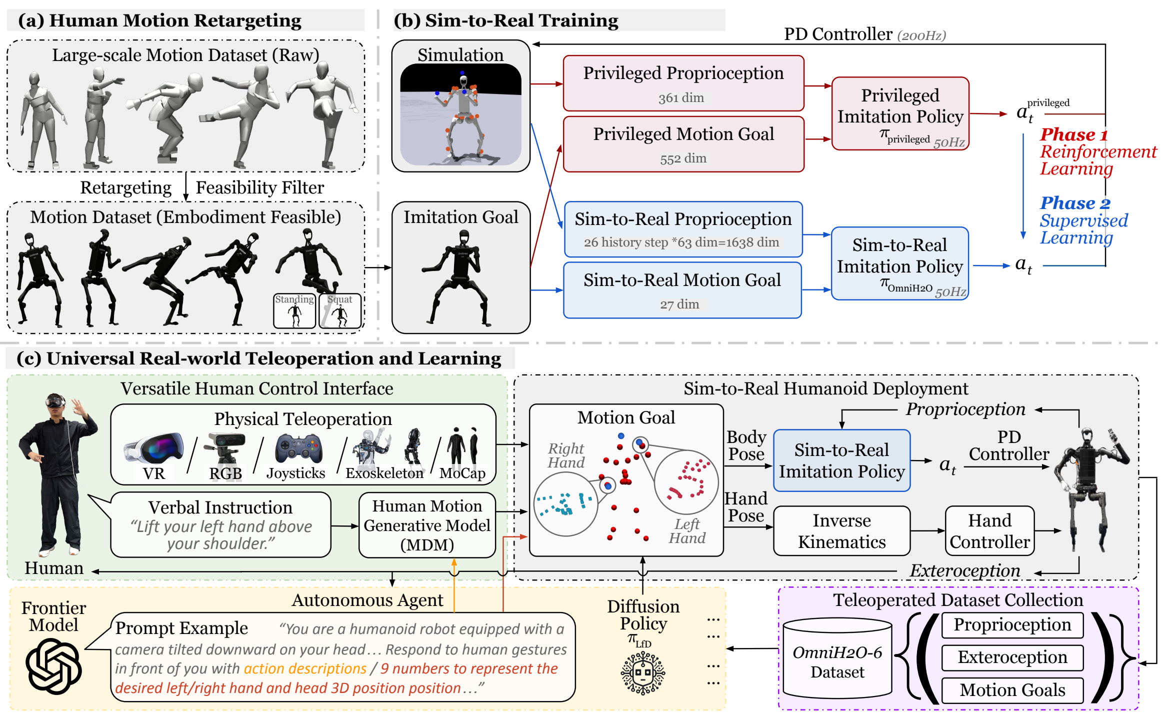
(a) Human Motion Retargeting
Large-scale Motion Dataset (Raw)
Retargeting
Feasibility Filter
Motion Dataset (Embodiment Feasible)
Standing
Squat
(b) Sim-to-Real Training
Simulation
Imitation Goal
PD Controller (200Hz)
Privileged Proprioception
361 dim
Privileged Motion Goal
552 dim
Privileged Imitation Policy
$\pi_{\text{privileged}}$ 50Hz
$a_t^{\text{privileged}}$
Phase 1
Reinforcement Learning
Phase 2
Supervised Learning
Sim-to-Real Proprioception
26 history step *63 dim=1638 dim
Sim-to-Real Motion Goal
27 dim
Sim-to-Real Imitation Policy
π_{OmniH2O} 50Hz
a_t
(c) Universal Real-world Teleoperation and Learning
Versatile Human Control Interface
Physical Teleoperation
VR
RGB
Joysticks
Exoskeleton
MoCap
Human
Verbal Instruction
"Lift your left hand above your shoulder."
Human Motion Generative Model (MDM)
Sim-to-Real Humanoid Deployment
Motion Goal
Right Hand
Left Hand
Body Pose
Hand Pose
Sim-to-Real Imitation Policy
a_t
PD Controller
Proprioception
Inverse Kinematics
Hand Controller
Exteroception
Autonomous Agent
Frontier Model
Prompt Example "You are a humanoid robot equipped with a camera tilted downward on your head… Respond to human gestures in front of you with action descriptions / 9 numbers to represent the desired left/right hand and head 3D position position…"
Diffusion Policy
π_{LfD}
Teleoperated Dataset Collection
OmniH2O-6 Dataset
Proprioception
Exteroception
Motion Goals

Fig. 2: (a) OmniH2O retargets large-scale human motions and filters out infeasible motions for humanoids. (b) Our **sim-to-real policy** is distilled through supervised learning from an **RL-trained teacher policy** using privileged information. (c) The universal design of OmniH2O supports versatile **human control interfaces** including VR headset, RGB camera, language, *etc.* Our system also supports to be controlled by **autonomous agents** like GPT-4o or imitation learning policy trained using our **dataset collected via teleoperation**.

TABLE I: Simulation motion imitation evaluation of OmniH2O and baselines.

			All sequences					Successful sequences			
Method	State Dimension	Sim2Real	Succ ↑	$E_{\text{g-mpjpe}}$ ↓	E_{mpjpe} ↓	E_{acc} ↓	E_{vel} ↓	$E_{\text{g-mpjpe}}$ ↓	E_{mpjpe} ↓	E_{acc} ↓	E_{vel} ↓
Privileged policy	$\mathcal{S} \subset \mathcal{R}^{913}$	✗	94.77%	126.51	70.68	3.57	6.20	122.71	69.06	2.22	5.20
H2O [12]	$\mathcal{S} \subset \mathcal{R}^{138}$	✓	87.52%	148.13	81.06	5.12	7.89	133.28	75.99	2.40	5.75
OmniH2O	$\mathcal{S} \subset \mathcal{R}^{1665}$	✓	**94.10%**	**141.11**	**77.82**	**3.70**	**6.54**	**135.49**	**75.75**	**2.30**	**5.47**
(a) Ablation on DAgger/RL											
OmniH2O-w/o-DAgger-History0	$\mathcal{S} \subset \mathcal{R}^{90}$	✗	90.62%	163.44	91.29	5.12	8.80	153.31	87.59	3.15	7.27
OmniH2O-w/o-DAgger	$\mathcal{S} \subset \mathcal{R}^{1665}$	✗	47.11%	223.27	128.90	15.03	16.29	182.13	119.54	5.47	9.10
OmniH2O-History0	$\mathcal{S} \subset \mathcal{R}^{90}$	✓	93.80%	141.21	78.52	3.74	6.62	**134.90**	76.11	**2.25**	5.48
OmniH2O	$\mathcal{S} \subset \mathcal{R}^{1665}$	✓	**94.10%**	**141.11**	**77.82**	**3.70**	**6.54**	135.49	**75.75**	2.30	**5.47**
(b) Ablation on History steps/Architecture											
OmniH2O-History50	$\mathcal{S} \subset \mathcal{R}^{3240}$	✓	93.56%	141.51	78.51	4.01	6.79	135.04	76.07	2.36	5.55
OmniH2O-History5	$\mathcal{S} \subset \mathcal{R}^{405}$	✓	93.60%	139.23	77.82	3.91	6.66	132.67	75.33	2.24	5.41
OmniH2O-History0	$\mathcal{S} \subset \mathcal{R}^{90}$	✓	93.80%	141.21	78.52	3.74	6.62	**134.90**	76.11	**2.25**	5.48
OmniH2O-GRU	$\mathcal{S} \subset \mathcal{R}^{90}$	✓	92.85%	147.67	80.84	4.05	6.93	142.75	79.10	2.38	5.66
OmniH2O-LSTM	$\mathcal{S} \subset \mathcal{R}^{90}$	✓	91.03%	147.36	80.34	4.12	7.04	142.64	78.59	2.37	5.72
OmniH2O-History25 (Ours)	$\mathcal{S} \subset \mathcal{R}^{1665}$	✓	**94.10%**	**141.11**	**77.82**	**3.70**	**6.54**	135.49	**75.75**	2.30	**5.47**
(c) Ablation on Tracking Points											
OmniH2O-22points	$\mathcal{S} \subset \mathcal{R}^{1836}$	✓	**94.72%**	**127.71**	**70.39**	**3.62**	**6.25**	**123.87**	**68.92**	**2.22**	**5.24**
OmniH2O-8points	$\mathcal{S} \subset \mathcal{R}^{1710}$	✓	94.31%	129.30	71.70	3.78	6.39	125.14	70.07	2.22	5.26
OmniH2O-3points (Ours)	$\mathcal{S} \subset \mathcal{R}^{1665}$	✓	94.10%	141.11	77.82	3.70	6.54	135.49	75.75	2.30	5.47
(d) Ablation on Linear Velocity											
OmniH2O-w-linvel	$\mathcal{S} \subset \mathcal{R}^{1743}$	✓	93.80%	**138.18**	78.12	3.94	6.61	**132.44**	75.98	**2.29**	**5.40**
OmniH2O	$\mathcal{S} \subset \mathcal{R}^{1665}$	✓	**94.10%**	141.11	**77.82**	**3.70**	**6.54**	135.49	**75.75**	2.30	5.47

on 20 standing sequences due to the limited physical lab space and the difficulty of evaluating on large-scale datasets in the real world. Detailed state-space composition (Section VII), ablation setup (Section VI), hyperparameters (Section XV), and hardware configuration (Section V) are summarized in the Appendix.

Metrics. We evaluate the motion tracking performance using both pose and physics-based metrics. We report Success rate (Succ) as in PHC [19], where imitation is unsuccessful if the average deviation from reference is farther than 0.5m at any point in time. Succ measures whether the humanoid can track the reference motion without losing balance or lagging behind. The global MPJPE $E_{g-\text{mpjpe}}$ and the root-relative mean per-joint position error (MPJPE) E_{mpjpe} (in mm) measures our policy's ability to imitate the reference motion globally and locally (root-relative). To show physical realism, we report average joint acceleration E_{acc} (mm/frame^2) and velocity E_{vel} (mm/frame) error.

1) Simulation Motion-Tracking Results: In Table I's first three rows, we can see that our deployable student policy significantly improves upon prior art [12] on motion imitation and achieves a similar success rate as the teacher policy.

Ablation on DAgger/RL. We test the performance of OmniH2O without DAgger (*i.e.*, directly using RL to train the student policy). In Table I(a) we can see that DAgger improves performance overall, especially for policy with history input. Without DAgger the policy struggles to learn a coherent policy when provided with a long history. This is due to RL being unable to handle the exponential growth in input complexity. However, the history information is necessary for learning a deployable policy in the real-world, providing robustness and implicit global velocity information (see Section XVIII-B). Supervised learning via DAgger is able to effectively leverage the history input and is able to achieve better performance.

Ablation on History Steps/Architecture. In Table I(b), we experiment with varying history steps (0, 5, 25, 50) and find that 25 steps achieve the best balance between performance and learning efficiency. Additionally, we evaluate different neural network architectures for history utilization: MLP, LSTM, GRU and determine that MLP-based OmniH2O performs the best. More experimental results and discussions are provided in Section XVIII

B. *Human Control via Universal Interfaces*

To answer **Q2**, we demonstrate real-world capabilities of OmniH2O with versatile human control interfaces. All the capabilities discussed below utilize the same policy.

Teleoperation. We teleoperate the humanoid using π_{OmniH2O} with both VR and RGB camera as interfaces. The results are

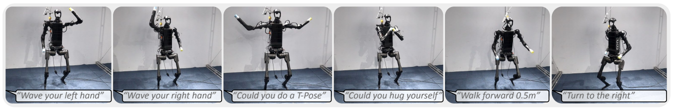

Fig. 3: OmniH2O policy tracks motion goals from a language-based human motion generative model [33].

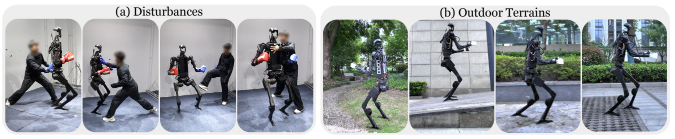

Fig. 4: OmniH2O shows superior robustness against human strikes and different outdoor terrains.

shown in Figure 9(a) and Section XIII, where the robot is able to finish dexterous loco-manipulation tasks with high precision and robustness.

Language Instruction Control. By linking π_{OmniH2O} with a pretrained text to motion generative model (MDM) [33], it enables controlling the humanoid via verbal instructions. As shown in Figure 3, with humans describing desired motions, such as "*raise your right hand*". MDM generates the corresponding motion goals that are tracked by the OmniH2O.

Robustness Test. As shown in Figure 4, we test the robustness of our control policy. We use the same policy π_{OmniH2O} across all tests, whether with fixed standing motion goals or motion goals controlled by joysticks, either moving forward or backward. With human punching and kicking from various angles, the robot, without external assistance, is able to maintain stability on its own. We also test OmniH2O on various outdoor terrains. OmniH2O demonstrates great robustness under disturbances and unstructured terrains.

C. Autonomy via Frontier Models or Imitation Learning

To answer **Q3**, we need to bridge the whole-body tracking policy (*physical intelligence*), with automated generation of kinematic motion goals through visual input (*semantic intelligence*). We explore two ways of automating humanoid control with OmniH2O: (1) using multi-modal frontier models to generate motion goals and (2) learning autonomous policies from the teleoperated dataset.

GPT-4o Autonomous Control. We integrate our system, OmniH2O, with GPT-4o, utilizing a head-mounted camera on the humanoid to capture images for GPT-4o (Figure 5). The prompt (details in Section XVII) provided to GPT-4o offers several motion primitives for it to choose from, based on the current visual context. We opt for motion primitives rather than directly generating motion goals because of GPT-4o's relatively long response time. As shown in Figure 5, the robot manages to give the correct punch based on the color of the target and successfully greets a human based on the intention indicated by human poses.

***OmniH2O-6* Dataset**. We collect demonstration data via VR-based teleoperation. We consider six tasks: Catch-Release, Squat, Rope-Paper-Scissors, Hammer-Catch, Boxing, and Pasket-Pick-Place. Our dataset includes paired RGBD images from the head-mounted camera, the motion goals of H1's head and hands with respect to the root, and joint targets for motor actuation, recorded at 30Hz. Detailed task descriptions of the

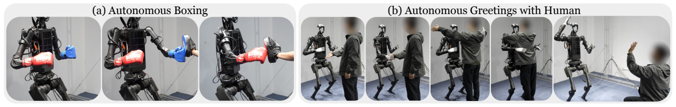

Fig. 5: OmniH2O sends egocentric RGB views to GPT-4o and executes the selected motion primitives.

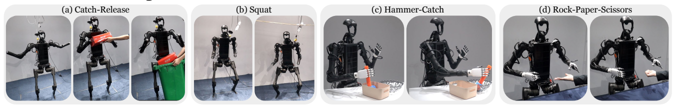

Fig. 6: OmniH2O autonomously conducts four tasks using LfD models trained with our collected data.

six open-sourced datasets are in Appendix XIV.

Humanoid Learning from Demonstrations. We design our learning from demonstration policy to be $\pi_{\text{LfD}}(\hat{\boldsymbol{p}}^{\text{Sparse-lfd}}_{t:t+\phi}|\boldsymbol{I}_t)$, where π_{LfD} outputs ϕ frames of motion goals given the image input $\boldsymbol{I}_t$. Here, we also include dexterous hand commands in $\hat{\boldsymbol{p}}^{\text{Sparse-lfd}}_{t:t+\phi}$. Then, our $\pi_{\text{OmniH2O}}(\boldsymbol{a}_t|\boldsymbol{s}^{\text{p-real}}_t, \boldsymbol{s}^{\text{g-real}}_t)$ serves as the low-level policy to compute joint actuations for humanoid whole-body control. The training hyperparameters are in Section XVI. Compared to directly using the π_{LfD} to output joint actuation, we leverage the trained motor skills in π_{OmniH2O}, which drastically reduces the number of demonstrations needed. We benchmark a variety of imitation learning algorithms on four tasks in our collected dataset (shown in Figure 6), including Diffusion Policy [4] with Denoising Diffusion Probabilistic Model [14] (DP-DDPM) and Denoising Diffusion Implicit Model [32] (DP-DDIM) and vanilla Behavior Cloning with a ResNet architecture (BC). Detailed descriptions of these methods are provided in Section VIII. To evaluate π_{LfD}, we report the average MSE loss and the success rate in Table II, where we average the metrics across all tasks. More details for each task evaluation can be found in Section XIV. We draw two key conclusions: (1) The Diffusion Policy significantly outperforms vanilla BC with ResNet; (2) In our LfD training, predicting a sequence of actions is crucial, as it enables the robot to effectively learn and replicate the trajectory.

TABLE II: Quantitative LfD average performance on 4 tasks over 10 runs.

Metrics	All Tasks		
(a) Ablation on Data size			
	25%data	50%data	100%data
MSE Loss	1.30E-2	7.48E-3	5.25E-4
Succ rate	4/10	6.5/10	8/10
(b) Ablation on Sequence observation/action			
	Si-O-Si-A	Se-O-Se-A	Si-O-Se-A
MSE Loss	4.89E-4	9.91E-4	5.25E-4
Succ rate	6.5/10	8.75/10	8/10
(c) Ablation on BC/DDIM/DDPM			
	BC	DP-DDIM	DP-DDPM
MSE Loss	5.63E-3	1.9E-3	5.25E-4
Succ rate	1/10	7.75/10	8/10

IV. Limitations and Future Work

Summary. OmniH2O enables dexterous whole-body humanoid loco-manipulation via teleoperation, designs universal control interfaces, facilitates scalable demonstration collection, and empowers humanoid autonomy via frontier models or humanoid learning from demonstrations.

Limitations. One limitation of our system is the requirement of robot root odometry to transfer pose estimation from teleoperation interfaces to motion goals in the robot frame. Results from VIO can be noisy or even discontinuous, causing the motion goals to deviate from desired control. Another limitation is safety; although the OmniH2O policy has shown great robustness, we do not have guarantees or safety checks for extreme disturbances or out-of-distribution motion goals (*eg.*, large discontinuity in motion goals).

References

[1] Josh Achiam, Steven Adler, Sandhini Agarwal, Lama Ahmad, Ilge Akkaya, Florencia Leoni Aleman, Diogo Almeida, Janko Altenschmidt, Sam Altman, Shyamal Anadkat, et al. Gpt-4 technical report. *arXiv preprint arXiv:2303.08774*, 2023.

[2] Luigi Campanaro, Siddhant Gangapurwala, Wolfgang Merkt, and Ioannis Havoutis. Learning and deploying robust locomotion policies with minimal dynamics randomization, 2023.

[3] Xuxin Cheng, Jialong Li, Shiqi Yang, Ge Yang, and Xiaolong Wang. Open-television: open-source teleoperation with vision, 2024.

[4] Cheng Chi, Siyuan Feng, Yilun Du, Zhenjia Xu, Eric Cousineau, Benjamin Burchfiel, and Shuran Song. Diffusion policy: Visuomotor policy learning via action diffusion. *arXiv preprint arXiv:2303.04137*, 2023.

[5] Damiao. Static, dynamic, fictitious, strong, 2018. URL https://www.mdmbot.com/.

[6] Jeremy Dao, Kevin Green, Helei Duan, Alan Fern, and Jonathan Hurst. Sim-to-real learning for bipedal locomotion under unsensed dynamic loads. In *2022 International Conference on Robotics and Automation (ICRA)*, pages 10449–10455. IEEE, 2022.

[7] Kourosh Darvish, Luigi Penco, Joao Ramos, Rafael Cisneros, Jerry Pratt, Eiichi Yoshida, Serena Ivaldi, and Daniele Pucci. Teleoperation of humanoid robots: A survey. *IEEE Transactions on Robotics*, 39(3):1706–1727, 2023.

[8] Helei Duan, Bikram Pandit, Mohitvishnu S Gadde, Bart Jaap van Marum, Jeremy Dao, Chanho Kim, and Alan Fern. Learning vision-based bipedal locomotion for challenging terrain. *arXiv preprint arXiv:2309.14594*, 2023.

[9] Zipeng Fu, Tony Z Zhao, and Chelsea Finn. Mobile aloha: Learning bimanual mobile manipulation with low-cost whole-body teleoperation. *arXiv preprint arXiv:2401.02117*, 2024.

[10] Ankur Handa, Karl Van Wyk, Wei Yang, Jacky Liang, Yu-Wei Chao, Qian Wan, Stan Birchfield, Nathan Ratliff, and Dieter Fox. Dexpilot: Vision-based teleoperation of dexterous robotic hand-arm system. In *2020 IEEE International Conference on Robotics and Automation (ICRA)*, pages 9164–9170. IEEE, 2020.

[11] Kensuke Harada, Shuuji Kajita, Hajime Saito, Mitsuharu Morisawa, Fumio Kanehiro, Kiyoshi Fujiwara, Kenji Kaneko, and Hirohisa Hirukawa. A humanoid robot carrying a heavy object. In *Proceedings of the 2005 IEEE International Conference on Robotics and Automation*, pages 1712–1717. IEEE, 2005.

[12] Tairan He, Zhengyi Luo, Wenli Xiao, Chong Zhang, Kris Kitani, Changliu Liu, and Guanya Shi. Learning human-to-humanoid real-time whole-body teleoperation. *arXiv preprint arXiv:2403.04436*, 2024.

[13] Tairan He, Chong Zhang, Wenli Xiao, Guanqi He, Changliu Liu, and Guanya Shi. Agile but safe: Learning collision-free high-speed legged locomotion. *arXiv preprint arXiv:2401.17583*, 2024.

[14] Jonathan Ho, Ajay Jain, and Pieter Abbeel. Denoising diffusion probabilistic models. *Advances in neural information processing systems*, 33:6840–6851, 2020.

[15] Inspire-robots. Smaller and higher-precision motion control experts, 2018. URL https://inspire-robots.store/.

[16] Joonho Lee, Jemin Hwangbo, Lorenz Wellhausen, Vladlen Koltun, and Marco Hutter. Learning quadrupedal locomotion over challenging terrain. *Science robotics*, 5 (47):eabc5986, 2020.

[17] Zhongyu Li, Xuxin Cheng, Xue Bin Peng, Pieter Abbeel, Sergey Levine, Glen Berseth, and Koushil Sreenath. Reinforcement learning for robust parameterized locomotion control of bipedal robots. In *2021 IEEE International Conference on Robotics and Automation (ICRA)*, pages 2811–2817. IEEE, 2021.

[18] Zhongyu Li, Xue Bin Peng, Pieter Abbeel, Sergey Levine, Glen Berseth, and Koushil Sreenath. Reinforcement learning for versatile, dynamic, and robust bipedal locomotion control. *arXiv preprint arXiv:2401.16889*, 2024.

[19] Zhengyi Luo, Jinkun Cao, AlexanderWinkler, Kris Kitani, and Weipeng Xu. Perpetual humanoid control for real-time simulated avatars. In *Proceedings of the IEEE/CVF International Conference on Computer Vision (ICCV)*, pages 10895–10904, October 2023.

[20] Naureen Mahmood, Nima Ghorbani, Nikolaus F Troje, Gerard Pons-Moll, and Michael J Black. Amass: Archive of motion capture as surface shapes. *Proceedings of the IEEE International Conference on Computer Vision*, 2019-Octob:5441–5450, 2019. ISSN 1550-5499.

[21] Federico L Moro and Luis Sentis. Whole-body control of humanoid robots. *Humanoid robotics: a reference*, pages 1161–1183, 2019.

[22] Masaki Murooka, Iori Kumagai, Mitsuharu Morisawa, Fumio Kanehiro, and Abderrahmane Kheddar. Humanoid loco-manipulation planning based on graph search and reachability maps. *IEEE Robotics and Automation Letters*, 6(2):1840–1847, 2021.

[23] Younghyo Park and Pulkit Agrawal. Using apple vision pro to train and control robots, 2024. URL https://github.com/Improbable-AI/VisionProTeleop.

[24] Ilija Radosavovic, Tete Xiao, Bike Zhang, Trevor Darrell, Jitendra Malik, and Koushil Sreenath. Real-world humanoid locomotion with reinforcement learning. *Science Robotics*, 9(89):eadi9579, 2024.

[25] Ilija Radosavovic, Bike Zhang, Baifeng Shi, Jathushan Rajasegaran, Sarthak Kamat, Trevor Darrell, Koushil Sreenath, and Jitendra Malik. Humanoid locomotion as next token prediction. *arXiv preprint arXiv:2402.19469*, 2024.

[26] Stephane Ross, Geoffrey J Gordon, and J Andrew Bagnell. A reduction of imitation learning and structured prediction to no-regret online learning. *arXiv preprint*

arXiv:1011.0686, 2010.

[27] Nikita Rudin, David Hoeller, Philipp Reist, and Marco Hutter. Learning to walk in minutes using massively parallel deep reinforcement learning, 2022.

[28] John Schulman, Filip Wolski, Prafulla Dhariwal, Alec Radford, and Oleg Klimov. Proximal policy optimization algorithms. *CoRR*, abs/1707.06347, 2017. URL http://arxiv.org/abs/1707.06347.

[29] Mingyo Seo, Steve Han, Kyutae Sim, Seung Hyeon Bang, Carlos Gonzalez, Luis Sentis, and Yuke Zhu. Deep imitation learning for humanoid loco-manipulation through human teleoperation. In *2023 IEEE-RAS 22nd International Conference on Humanoid Robots (Humanoids)*, pages 1–8. IEEE, 2023.

[30] Kenneth Shaw, Ananye Agarwal, and Deepak Pathak. Leap hand: Low-cost, efficient, and anthropomorphic hand for robot learning. *arXiv preprint arXiv:2309.06440*, 2023.

[31] Jonah Siekmann, Yesh Godse, Alan Fern, and Jonathan Hurst. Sim-to-real learning of all common bipedal gaits via periodic reward composition. In *2021 IEEE International Conference on Robotics and Automation (ICRA)*, pages 7309–7315. IEEE, 2021.

[32] Jiaming Song, Chenlin Meng, and Stefano Ermon. Denoising diffusion implicit models. *arXiv preprint arXiv:2010.02502*, 2020.

[33] Guy Tevet, Sigal Raab, Brian Gordon, Yonatan Shafir, Daniel Cohen-Or, and Amit H. Bermano. Human motion diffusion model, 2022.

[34] Unitree. Unitree's first universal humanoid robot, 2018. URL https://www.unitree.com/h1.

Appendix

More real-world experiment videos are at the website https://omni.human2humanoid.com.

V. Real Robot System Setup

Our real robot employs a Unitree H1 platform [34], outfitted with Damiao DM-J4310-2EC motors [5] and Inspire hands [15] for its manipulative capabilities. We have two versions of real robot computing setup. (1) The first one has two 16GB Orin NX computers mounted on the back of the H1 robot. The first Orin NX is connected to a ZED camera mounted on the waist of H1, which performs computations to determine H1's own location for positioning. The camera operates at 60 Hz FPS. Additionally, this Orin NX connects via Wi-Fi to our Vision Pro device to continuously receive motion goal information from a human operator. The second Orin NX serves as our main control hub. It receives the motion goal information, which it uses as input for our control policy. This policy then outputs torque information for each of the robot's motors and sends these commands to the robot. As control for the robot's fingers and wrists does not require inference, it is directly mapped from the Vision Pro data to the corresponding joints on the robot. The policy's computation frequency is set at 50 Hz. The two Orin NX units are connected via Ethernet, sharing information through a common ROS (Robot Operating System) network. The final commands to H1 are consolidated and dispatched by the second Orin NX. Our entire system has a low latency of only 20 milliseconds. It's worth noting that we designed the system in this way partly because the ZED camera requires substantial computational resources. By dedicating the first Orin NX to the ZED camera, and the second to policy inference, we ensure that each component operates with optimal performance. (2) In the second setup, a laptop (13th Gen i9-13900HX and NVIDIA RTX4090, 32GB RAM) serves as the computing and communication device. All devices, including the ZED camera, control policy, and Vision Pro, communicate through this laptop on its ROS system, facilitating centralized data handling and command dispatch. These two setups yield similar performance, and we use them interchangeably in our experiments.

VI. Simulation Baseline and Ablations

In this section, we provide an explanation of each ablation method. **Main results in Table I**

- **Privileged policy**: This teacher policy $\pi_{\text{privileged}}$ incorporates all privileged environment information, along with complete motion goal and proprioception data in the observations. State space composition details in Table III.
- **H2O**: A policy trained using RL without DAgger and historical data, utilizing 8 keypoints of motion goal in observations. State space composition details in Table IV.
- **OmniH2O**: Our deployment policy π_{OmniH2O} that includes historical information and uses 3 keypoints of motion goal in observations, trained with DAgger. State space composition details in Table V.

Ablation on DAgger/RL in Table I(a)

- **OmniH2O-w/o-DAgger-History0**: This variant of OmniH2O is trained solely using RL and does not incorporate historical information within observations. State space composition details in Table VI.
- **OmniH2O-w/o-DAgger**: This model is trained using RL, excludes DAgger, but includes historical information from the last 25 steps in observations. State space composition details in Table VII.
- **OmniH2O-History0**: This model is trained with DAgger, but excludes historical information from the last 25 steps in observations. State space composition details in Table VIII.
- **OmniH2O**: This model is trained with DAgger and incorporates 25-step historical information within observations. State space composition details in Table V.

Ablation on History steps/Architecture in Table I(b)

- **OmniH2O-History50/25/5/0**: This variant of the OmniH2O with 50, 25, or 0 steps of historical information in the observations. State space composition details in Table IX.
- **OmniH2O-GRU/LSTM**: This version replaces the MLP in the policy network with either GRU or LSTM, inherently incorporating historical observations. State space composition details in Table X.

Ablation on Tracking Points in Table I(c)

- **OmniH2O-22/8/3points**: This variant of the OmniH2O policy includes 22, 8, or 3 keypoints of motion goal in the observations, with the 3 keypoints setting corresponding to the standard OmniH2O policy. State space composition details in Tables V, XI and XII.

Ablation on Linear Velocity in Table I(d)

- **OmniH2O-w-linvel**: This variant is almost the same as OmniH2O but with root linear velocity in observations and past linear velocity in history information. State space composition details in Table XIII.

VII. State Space Compositions

In this section, we introduce the detailed state space composition of baselines in the experiments.

Privileged Policy. This policy $\pi_{\text{privileged}}$ is the teacher policy that has access to all the available states for motion imitation, trained using RL.

TABLE III: State space information in Privileged Policy setting

State term	Dimensions
Motion goal DoF position	66
Motion goal DoF rotation	138
Motion goal DoF velocity	69
Motion goal DoF angular velocity	69
DoF position difference	69
DoF rotation difference	138
DoF velocity difference	69
DoF angular velocity difference	69
Local DoF position	69
Local DoF rotation	138
Actions	19
Total dim	913

H2O. This policy has 8 keypoints input (shoulder, elbow, hand, leg) and with global linear velocity, trained using RL.

TABLE IV: State space information in H2O setting

State term	Dimensions
DoF position	19
DoF velocity	19
Base velocity	3
Base angular velocity	3
Base gravity	3
Motion goal	72
Actions	19
Total dim	138

OmniH2O. This is our deployment policy π_{OmniH2O} with 25 history steps and without global linear velocity, trained using DAgger.

TABLE V: State space information in OmniH2O setting

State term	Dimensions
DoF position	19
DoF velocity	19
Base angular velocity	3
Base gravity	3
Motion goal	27
Actions	19
Single step total dim	90
History state term	Dimensions
DoF position	19
DoF velocity	19
Base angular velocity	3
Base gravity	3
Actions	19
History Single step total dim	63
Total dim	1665(63*25 + 90)

OmniH2O-w/o-DAgger-History0. This policy has a history of 0 steps, trained using RL.

TABLE VI: State space information in OmniH2O-w/o-DAgger-History0 setting

State term	Dimensions
DoF position	19
DoF velocity	19
Base angular velocity	3
Base gravity	3
Motion goal	27
Actions	19
Total dim	90

OmniH2O-w/o-DAgger. This policy has the same architecture as OmniH2O but trained with RL.

TABLE VII: State space information in OmniH2O-w/o-DAgger setting

State term	Dimensions
DoF position	19
DoF velocity	19
Base angular velocity	3
Base gravity	3
Motion goal	27
Actions	19
Single step total dim	90
History state term	Dimensions
DoF position	19
DoF velocity	19
Base angular velocity	3
Base gravity	3
Actions	19
History Single step total dim	63
Total dim	1665(63*25 + 90)

OmniH2O-History0. This policy has a history of 0 steps, trained using DAgger.

TABLE VIII: State space information in OmniH2O-History0 setting

State term	Dimensions
DoF position	19
DoF velocity	19
Base angular velocity	3
Base gravity	3
Motion goal	27
Actions	19
Total dim	90

OmniH2O-History$x$. This policy has a history of x steps, trained using DAgger.

TABLE IX: State space information in OmniH2O-History$x$ setting

State term	Dimensions
DoF position	19
DoF velocity	19
Base angular velocity	3
Base gravity	3
Motion goal	27
Actions	19
Single step total dim	90
History state term	Dimensions
DoF position	19
DoF velocity	19
Base angular velocity	3
Base gravity	3
Actions	19
History Single step total dim	63
Total dim	63*x + 90

OmniH2O-GRU/LSTM. This policy uses GRU/LSTM-based architecture, trained using DAgger.

TABLE X: State space information in OmniH2O-GRU/LSTM setting

State term	Dimensions
DoF position	19
DoF velocity	19
Base angular velocity	3
Base gravity	3
Motion goal	27
Actions	19
Total dim	90

OmniH2O-22points. This policy has 22 keypoints input (every joint on the humanoid), trained using DAgger.

TABLE XI: State space information in OmniH2O-22points setting

State term	Dimensions
DoF position	19
DoF velocity	19
Base angular velocity	3
Base gravity	3
Motion goal	198
Actions	19
Single step total dim	261
History state term	Dimensions
DoF position	19
DoF velocity	19
Base angular velocity	3
Base gravity	3
Actions	19
History Single step total dim	63
Total dim	1836(63*25+261)

OmniH2O-8points. This policy has 8 keypoints input (shoulder, elbow, hand, leg), trained using DAgger.

TABLE XII: State space information in OmniH2O-8points setting

State term	Dimensions
DoF position	19
DoF velocity	19
Base angular velocity	3
Base gravity	3
Motion goal	72
Actions	19
Single step total dim	135
History state term	Dimensions
DoF position	19
DoF velocity	19
Base angular velocity	3
Base gravity	3
Actions	19
History Single step total dim	63
Total dim	1710(63*25+135)

OmniH2O-w-linvel. This policy has 25 history steps and global linear velocity, trained using DAgger.

TABLE XIII: State space information in OmniH2O-w-linvel setting

State term	Dimensions
DoF position	19
DoF velocity	19
Base velocity	3
Base angular velocity	3
Base gravity	3
Motion goal	27
Actions	19
Single step total dim	93
History state term	Dimensions
DoF position	19
DoF velocity	19
Base velocity	3
Base angular velocity	3
Base gravity	3
Actions	19
History Single step total dim	66
Total dim	1743(66*25 + 93)

VIII. LfD Baselines

We conduct numerous ablation studies on LfD, aiming to benchmark the impact of various aspects on LfD tasks. The details of each ablation are as follows:

Ablation on Dataset size.

- 25/50/100% data: In this task, we use 25/50/100% of the dataset as the training set. The algorithm is DDPM which takes a single-step image as input and outputs 8 steps of actions.

Ablation on Single/Sequence observation/action input/output.

- Si-O-Si-A: Single-step observation and single-step action mean that we take 1 step of image data as input and predict 1 step of action as output.
- Se-O-Se-A: Sequence-steps observation and sequence-steps actions mean that we take 4 steps of image data as input and predict 8 steps of action as output.
- Si-O-Se-A: Single-step observation and sequence-steps actions mean that we take 1 step of image data as input and predict 8 steps of action as output.

Ablation on Training Architecture..

- BC: Behavior cloning which means we use resnet+MLP to predict the next 8 steps action from the current step's image.
- DP-DDIM: We use DDIM as the algorithm which takes a single-step image as input and outputs 8 steps of actions.
- DP-DDPM: We use DDPM as the algorithm which takes a single-step image as input and outputs 8 steps of actions.

IX. Reward Functions

Reward Components. Detailed reward components are summarized in Table XIV.

TABLE XIV: Reward components and weights: penalty rewards for preventing undesired behaviors for sim-to-real transfer, regularization to refine motion, and task reward to achieve successful whole-body tracking in real-time.

Term	Expression	Weight
	Penalty	
Torque limits	$\mathbb{1}(\boldsymbol{\tau}_t \notin [\boldsymbol{\tau}_{\min}, \boldsymbol{\tau}_{\max}])$	-2
DoF position limits	$\mathbb{1}(\boldsymbol{d}_t \notin [\boldsymbol{q}_{\min}, \boldsymbol{q}_{\max}])$	-125
DoF velocity limits	$\mathbb{1}(\dot{\boldsymbol{d}}_t \notin [\dot{\boldsymbol{q}}_{\min}, \dot{\boldsymbol{q}}_{\max}])$	-50
Termination	$\mathbb{1}_{\text{termination}}$	-250
	Regularization	
DoF acceleration	$\|\ddot{\boldsymbol{d}}_t\|_E 2$	-0.000011
DoF velocity	$\|\dot{\boldsymbol{d}}_t\|_2^2$	-0.004
Lower-body action rate	$\|\boldsymbol{a}_t^{\text{lower}} - \boldsymbol{a}_{t-1}^{\text{lower}}\|_2^2$	-3
Upper-body action rate	$\|\boldsymbol{a}_t^{\text{upper}} - \boldsymbol{a}_{t-1}^{\text{upper}}\|_2^2$	-0.625
Torque	$\|\boldsymbol{\tau}_t\|$	-0.0001
Feet air time	$T_{\text{air}} - 0.25$ [27]	1000
Max feet height for each step	$\max\{\boldsymbol{h}_{\text{max feet height for each step}} - 0.25, 0\}$	1000
Feet contact force	$\|F_{\text{feet}}\|_2^2$	-0.75
Stumble	$\mathbb{1}(F_{\text{feet}}^{xy} > 5 \times F_{\text{feet}}^{z})$	-0.00125
Slippage	$\|\boldsymbol{v}_t{}^{\text{feet}}\|_2^2 \times \mathbb{1}(F_{\text{feet}} \geq 1)$	-37.5
Feet orientation	$\|\boldsymbol{g}_z^{\text{feet}}\|$	-62.5
In the air	$\mathbb{1}(F_{\text{feet}}^{\text{left}}, F_{\text{feet}}^{\text{right}} < 1)$	-200
Orientation	$\|\boldsymbol{g}_z^{\text{root}}\|$	-200
	Task Reward	
DoF position	$\exp(-0.25\|\hat{\boldsymbol{d}}_t - \boldsymbol{d}_t\|_2)$	32
DoF velocity	$\exp(-0.25\|\hat{\dot{\boldsymbol{d}}}_t - \dot{\boldsymbol{d}}_t\|_2^2)$	16
Body position	$\exp(-0.5\|\boldsymbol{p}_t - \hat{\boldsymbol{p}}_t\|_2^2)$	30
Body position VRpoints	$\exp(-0.5\|\boldsymbol{p}_t^{\text{real}} - \hat{\boldsymbol{p}}_t^{\text{real}}\|_2^2)$	50
Body rotation	$\exp(-0.1\|\boldsymbol{\theta}_t \ominus \hat{\boldsymbol{\theta}}_t\|)$	20
Body velocity	$\exp(-10.0\|\boldsymbol{v}_t - \hat{\boldsymbol{v}}_t\|_2)$	8
Body angular velocity	$\exp(-0.01\|\boldsymbol{\omega}_t - \hat{\boldsymbol{\omega}}_t\|_2)$	8

Reward Curriculum. We have modified the cumulative discounted reward expression to handle multiple small rewards at each time step differently, depending on their sign. The revised formula is given by: $\mathbb{E}\left[\sum_{t=1}^{T}\gamma^{t-1}\sum_i s_{t,i} r_{t,i}\right]$ where $r_{t,i}$ represents different reward functions at time t, and $s_{t,i}$ is the scaling factor for each reward, defined as: $s_{t,i} = \begin{cases} s_{\text{current}} & \text{if } r_{t,i} < 0 \\ 1 & \text{if } r_{t,i} \geq 0 \end{cases}$ where $s_{current}$ is the scaling factor. This scaling factor is adjusted dynamically: it is multiplied by 0.9999 when the average episode length is less than 40, and multiplied by 1.0001 when it exceeds 120. The init $s_{current}$ is set to 0.5, then the upper bound of this scaling factor is set to 1. This modification allows our policy to progressively learn from simpler to more complex scenarios with higher penalties, thereby reducing the difficulty for RL in exploring the optimal policy.

X. Domain Randomizations

Detailed domain randomization setups are summarized in Table XV.

TABLE XV: Here we describe the range of dynamics randomization for simulated dynamics randomization, external perturbation, and terrain, which are important for sim-to-real transfer, robustness, and generalizability.

Term	Value
Dynamics Randomization	
Friction	$\mathcal{U}(0.2, 1.1)$
Base CoM offset	$\mathcal{U}(-0.1, 0.1)$m
Link mass	$\mathcal{U}(0.7, 1.3) \times$ default kg
P Gain	$\mathcal{U}(0.75, 1.25) \times$ default
D Gain	$\mathcal{U}(0.75, 1.25) \times$ default
Torque RFI [2]	$0.1 \times$ torque limit $\text{N} \cdot \text{m}$
Control delay	$\mathcal{U}(20, 60)$ms
Motion reference offset	$\mathcal{U}([-0.02, 0.02], [-0.02, 0.02], [-0.1, 0.1])$cm
External Perturbation	
Push robot	interval $= 5s$, $v_{xy} = 1$m/s
Randomized Terrain	
Terrain type	flat, rough, low obstacles [13]

XI. Linear Velocity Estimation

The illustration of using the ZED camera VIO module and the comparison of VIO with neural state estimators are shown in Figure 7. We train our neural velocity estimators using a supervised learning approach. The process involves repeatedly deploying our policy in simulation with different motion goals. In every environment step, we use the root linear velocity to supervise our velocity estimator.

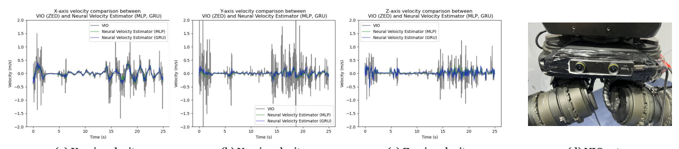

(a) X-axis velocity (b) Y-axis velocity (c) Z-axis velocity (d) VIO setup

Fig. 7: The illustration of using ZED camera VIO module, and the comparison of the velocity estimation of VIO with neural state estimators.

XII. Ablation on Dataset Motion Distribution

The ablation study on motion data distribution is shown in Figure 8. The policy trained without motion data augmentation is hard to stand still and make upper-body moves.

XIII. Additional Physical Teleoperation Results

Additional VR-based and RGB-based teleoperation demo are shown in Figure 10.

XIV. Dataset and Imitation Learning

As shown in Figure 11, we collected 6 LfD tasks' dataset to enable the robot to autonomously perform certain functions.
Catch-Release: Catch a red box and release it into a trash bin. This task has 13234 frames in total.
Squat: Squat when the robot sees a horizontal bar approaching that is lower than its head height. This task has 8535 frames in total.
Hammer-Catch: Use right hand to catch a hammer in a box. This task has 12759 frames in total.
Rock-Paper-Scissors: When the robot sees the person opposite it makes one of the rock-paper-scissors gestures, it should respond with the corresponding gesture that wins. This task has 9380 frames in total.
Boxing: When you see a blue boxing target, throw a left punch; when you see a red one, throw a right punch. This task has 11118 frames in total.
Basket-Pick-Place: Use your right hand to pick up the box and place it in the middle when the box is on the right side, and use your left hand if the box is on the left side. If you pick up the box with your right hand, place it on the left side using your left hand; if picked up with your left hand, place it on the right side using your right hand. This task has 18436 frames in total.

The detailed performance of 4 tasks is documented in Table XVI

TABLE XVI: Quantitative LfD autonomous agents performance for 4 tasks.

Metrics	Catch-Release			Squat			Hammer-Catch			Rock-Paper-Scissors		
(a) Ablation on Data size												
	25%data	50%data	100%data	25%data	50%data	100%data	25%data	50%data	100%data	25%data	50%data	100%data
MSE Loss	3.01E-3	3.04E-4	9.89E-5	1.25E-4	1.10E-4	7.07E-5	2.18E-2	1.56E-2	3.29E-4	2.72E-2	1.39E-2	1.60E-3
Succ rate	1/10	3/10	6/10	9/10	10/10	10/10	3/10	6/10	6/10	3/10	9/10	10/10
(b) Ablation on Sequence observation/action												
	Si-O-Si-A	Se-O-Se-A	Si-O-Se-A	Si-O-Si-A	Se-O-Se-A	Si-O-Se-A	Si-O-Si-A	Se-O-Se-A	Si-O-Se-A	Si-O-Si-A	Se-O-Se-A	Si-O-Se-A
MSE Loss	2.52E-4	1.47E-4	9.89E-5	5.18E-5	9.60E-5	7.07E-5	2.22E-4	3.62E-4	3.29E-4	1.43E-3	3.36E-3	1.60E-3
Succ rate	3/10	7/10	6/10	10/10	10/10	10/10	5/10	9/10	6/10	10/10	9/10	10/10
(c) Ablation on BC/DDIM/DDPM												
	BC	DP-DDIM	DP-DDPM	BC	DP-DDIM	DP-DDPM	BC	DP-DDIM	DP-DDPM	BC	DP-DDIM	DP-DDPM
MSE Loss	1.39E-3	4.79E-5	9.89E-5	6.24E-4	6.42E-5	7.07E-5	4.50E-3	3.41E-4	3.29E-4	1.46E-2	2.42E-3	1.60E-3
Succ rate	0/10	6/10	6/10	3/10	10/10	10/10	0/10	5/10	6/10	1/10	10/10	10/10

XV. Sim2real Training Hyperparameters

The hyperparameters for our RL/DAgger policy training are detailed in Table XVII below.

TABLE XVII: Hyperparameters

Hyperparameters	Values
Batch size	64
Discount factor (γ)	0.99
Learning rate	0.001
Clip param	0.2
Entropy coef	0.005
Max grad norm	0.2
Value loss coef	1
Entropy coef	0.005
Init noise std (RL)	1.0
Init noise std (DAgger)	0.001
Num learning epochs	5
MLP size	[512, 256, 128]

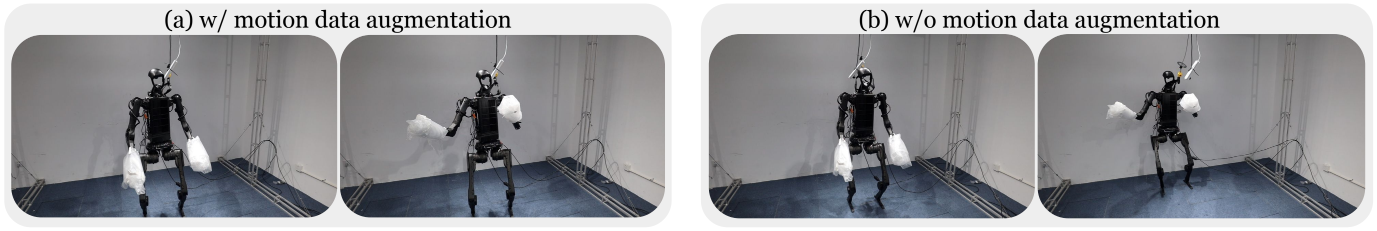
(a) w/ motion data augmentation
(b) w/o motion data augmentation

Fig. 8: The ablation of data augmentation.

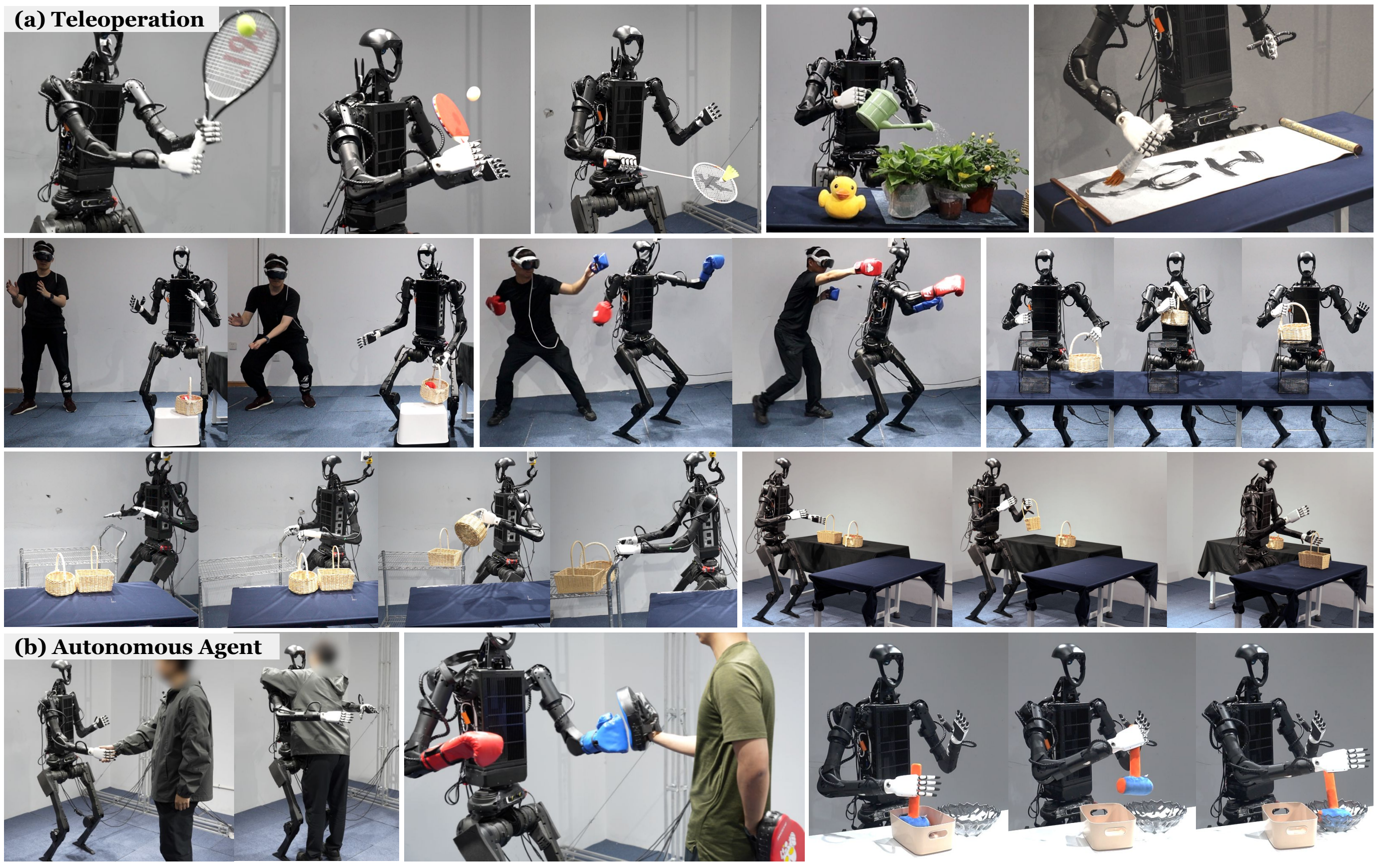

Fig. 9: (a) OmniH2O enables teleoperating a full-size humanoid robot (Unitree H1) to complete tasks that require both high-precision manipulation and locomotion. (b) OmniH2O also enables full autonomy through visual input, controlled by GPT-4o or a policy learned from teleoperated demonstrations. **Videos**: see our website: https://omni.human2humanoid.com

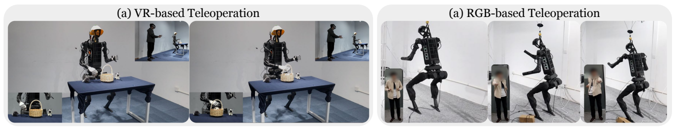

Fig. 10: More physical teleoperation showcases.

XVI. LfD Hyperparameters

In order to make the robot autonomous, we have developed a Learning from Demonstration (LfD) approach utilizing a diffusion policy that learns from a dataset we collected. The default training hyperparameters are shown below in Table XVIII.

TABLE XVIII: Training Hyperparameters for the Lfd Training

Hyperparameter	**Default Value**
Batch Size	32
Observation Horizon	1
Action Horizon	8
Prediction Horizon	16
Policy Dropout Rate	0.0
Dropout Rate (State Encoder)	0.0
Image Dropout Rate	0.0
Weight Decay	1E-5
Image Output Size	32
State Noise	0.0
Image Gaussian Noise	0.0
Image Masking Probability	0.0
Image Patch Size	16
Number of Diffusion Iterations	100

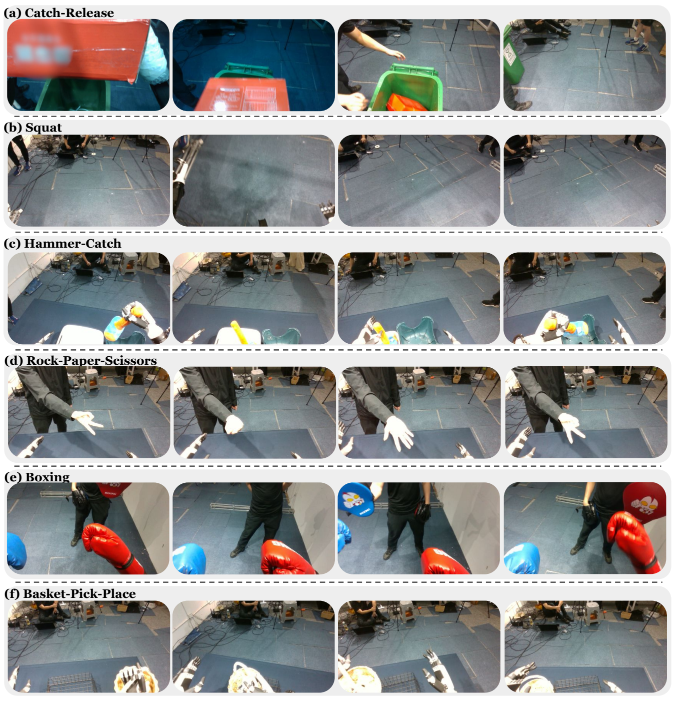

Fig. 11: *OmniH2O-6* dataset.

XVII. GPT-4o Prompt Example

Here is the example prompt we use for **Autonomous Boxing** task:

You're a humanoid robot equipped with a camera slightly tilted downward on your head, providing a first-person perspective. I am assigning you a task: when a blue target appears in front of you, extend and then retract your left fist. When a red target appears, do the same with your right fist. If there is no target in front, remain stationary. I will provide you with three options each time: move your left hand forward, move your right hand forward, or stay motionless. You should directly respond with the corresponding options A, B, or C based on the current image. Note that, yourself is also wearing blue left boxing glove and right red boxing glove, please do not recognize them as the boxing target. Now, based on the current image, please provide me with the A, B, C answers.

For **Autonomous Greetings with Human** Task, our prompt is:

You are a humanoid robot equipped with a camera slightly tilted downward on your head, providing a first-person perspective. I am assigning you a new task to respond to human gestures in front of you. Remember, the person is standing facing you, so be mindful of their gestures. If the person extends their right hand to shake hands with you, use your right hand to shake their right hand (Option A). If the person opens both arms wide for a hug, open your arms wide to reciprocate the hug (Option B). If you see the person waving his hand as a gesture to say goodbye, respond by waving back (Option C). If no significant gestures are made, remain stationary (Option D). Respond directly with the corresponding options A, B, C, or D based on the current image and observed gestures. Directly reply with A, B, C, or D only, without any additional characters.

It is worth mentioning that we can use GPT-4 not only to choose motion primitive but also to directly generate the motion goal. The following prompt exemplifies this process:

You are a humanoid robot equipped with a camera slightly tilted downward on your head, providing a first-person perspective. I am assigning you a new task to respond to human gestures in front of you. If the person extends his left hand for a handshake, extend your left hand to reciprocate. If they extend their right hand, respond by extending your right hand. If the person opens both arms wide for a hug, open your arms wide to reciprocate the hug. If no significant gestures are made, remain stationary. Respond 6 numbers to represent the desired left and right hand 3D position with respect to your root position. For example: [0.25, 0.2, 0.3, 0.15, -0.19, 0.27] means the desired position of the left hand is 0.25m forward, 0.2m left, and 0.3m high compared to pelvis position, and the desired position of the right hand is 0.15m forward, 0.19m right and 0.27m high compared to pelvis position. The default stationary position should be (0.2, 0.2, 0.2, 0.2, -0.2, 0.2). Now please respond the 6d array based on the image to respond to the right hand shaking, left hand shaking, and hugging.

XVIII. More Experimental Results

A. Simulation Results

Ablation on Sparse Input. To support VR-based teleoperation, π_{OmniH2O} only tracks 3-points (head and hands) to produce whole-body motion. The impact of the number of tracking points is examined in Table I(c). We test configurations ranging from minimal (3) to full-body motion goal (22) and found that 3-point tracking can achieve comparable performance with more input keypoints. As expected, 3-point policy sacrifices some whole-body motion tracking accuracy but gains greater applicability to commercially available devices.

Ablation on Global Linear Velocity. Given the challenges associated with global velocity estimation in real-world applications, we compare policies trained with and without explicit velocity information. In Table I(d), we find that linear velocity information does not boost performance in simulation, but it introduces significant challenges in real-world deployment (details illustrated in Section XVIII-B), prompting us to develop a policy with state spaces that do not depend on linear velocity as proprioception to avoid these issues.

B. Real-world Motion-Tracking Results

Ablation on Real-world Linear Velocity Estimation. We exclude linear velocity in our state space design global linear velocity obtained by algorithms such as visual inertial odometry (VIO) can be rather noisy, as shown in Section XI. Our ablation study (Table XIX(a)) also shows that policies without velocity input has better performance compared with policies using velocities estimated by VIO or MLP/GRU neural estimators (implementation details in Section XI), which suggests that the policy with history can effectively track motions without explicit linear velocity as input.

TABLE XIX: Real-world motion tracking evaluation on 20 standing motions in $\hat{\boldsymbol{Q}}$

		Tested sequences			
Method	State Dimensions	$E_{\text{g-mpjpe}} \downarrow$	$E_{\text{mpjpe}} \downarrow$	$\text{E}_{\text{acc}} \downarrow$	$\text{E}_{\text{vel}} \downarrow$
H2O [12]	$\mathcal{S} \subset \mathcal{R}^{138}$	87.33	53.32	6.03	5.87
OmniH2O	$\mathcal{S} \subset \mathcal{R}^{1665}$	**47.94**	**41.87**	**1.84**	**2.20**
(a) Ablation on Real-world Linear Velocity estimation					
OmniH2O-w-linvel(VIO)[1,2]	$\mathcal{S} \subset \mathcal{R}^{1743}$	N/A	N/A	N/A	N/A
OmniH2O-w-linvel(MLP)	$\mathcal{S} \subset \mathcal{R}^{1743}$	50.93	42.47	2.16	2.26
OmniH2O-w-linvel(GRU)	$\mathcal{S} \subset \mathcal{R}^{1743}$	49.75	42.38	2.20	2.31
OmniH2O	$\mathcal{S} \subset \mathcal{R}^{1665}$	**47.94**	**41.87**	**1.84**	**2.20**
(b) Ablation on History steps/Architecture					
OmniH2O-History0	$\mathcal{S} \subset \mathcal{R}^{90}$	83.26	46.00	4.86	4.45
OmniH2O-History5	$\mathcal{S} \subset \mathcal{R}^{405}$	62.18	46.50	2.66	2.90
OmniH2O-History50	$\mathcal{S} \subset \mathcal{R}^{3240}$	50.24	**40.11**	2.37	2.71
OmniH2O-LSTM	$\mathcal{S} \subset \mathcal{R}^{90}$	87.00	46.06	3.89	3.88
OmniH2O	$\mathcal{S} \subset \mathcal{R}^{1665}$	**47.94**	41.87	**1.84**	**2.20**

[1] Use ZED SDK to estimate the linear velocity.
[2] Unable to finish the real-world test due to falling on the ground.

History Steps and Architecture. Real-world evaluation in Table XIX(b) also shows that our choice of 25 steps of history achieves the best performance. The tracking performance of LSTM shows that MLP-based policy performs better in the real-world.